Electric Sail-Based Displaced Orbits with a Refined Thrust Model

Lorenzo Niccolai, Alessandro A. Quarta*, Giovanni Mengali

Department of Civil and Industrial Engineering, University of Pisa, I-56122 Pisa, Italy

Abstract

This paper analyzes the performance of an electric solar wind sail for generating and maintaining a heliocentric circular displaced orbit. Previous research on this subject was based on a simplified mathematical model of the spacecraft thrust. However, recent studies have proposed a more accurate algorithm for evaluating both the modulus and the direction of the propulsive thrust as a function of some important parameters related to the spacecraft attitude. Therefore, a reappraisal of the problem is motivated by the need of revising the past results taking into account the new information available on the propulsion system. Within this context, the paper focuses on circular displaced orbits that are characterized in terms of orbital period, heliocentric distance and elevation angle. The attitude configuration and the value of the spacecraft characteristic acceleration required for orbital maintenance are calculated. An in depth analysis of the linear stability of displaced orbits is given. It is shown that displaced orbits are unstable when the elevation angle exceeds about $20\,\mathrm{deg}$.

Keywords: Electric solar wind sail, displaced non-Keplerian orbits, mission analysis, deep space missions, propellantless propulsion systems

Nomenclature

$\boldsymbol{a}$	=	propulsive acceleration vector (with $a \triangleq \|\boldsymbol{a}\|$), $[\mathrm{mm/s^2}]$
a_c	=	spacecraft characteristic acceleration, $[\mathrm{mm/s^2}]$
$\hat{\boldsymbol{i}}$, $\hat{\boldsymbol{j}}$, $\hat{\boldsymbol{k}}$	=	Cartesian heliocentric reference frame unit vectors
$\hat{\boldsymbol{n}}$	=	unit vector normal to the E-sail mean plane
O	=	Sun's center-of-mass
$\mathcal{P}$	=	E-sail nominal plane
$\boldsymbol{r}$	=	position vector (with $r \triangleq \|\boldsymbol{r}\|$), [au]
$r_\oplus$	=	reference distance (1 au)
r_l	=	hovering distance, [au]
$\mathcal{R}$	=	local horizontal plane
S	=	spacecraft center-of-mass
T	=	orbital period [years]
$\boldsymbol{v}$	=	velocity vector, [km/s]
α	=	cone angle [deg]
α_n	=	pitch angle [deg]
γ	=	dimensionless propulsive acceleration
δ	=	clock angle [deg]
δ_n	=	azimuthal angle [deg]
$\mu_\odot$	=	Sun's gravitational parameter, $[\mathrm{km^3/s^2}]$

*Corresponding author

Email addresses: lorenzoniccolai88@gmail.com (Lorenzo Niccolai), a.quarta@ing.unipi.it (Alessandro A. Quarta), g.mengali@ing.unipi.it (Giovanni Mengali)

Published in Proc IMechE, Part G: Journal of Aerospace Engineering, online before print, 2016. doi: 10.1177/0954410016679195

$\hat{\boldsymbol{\rho}}$ = radial unit vector
ρ = radius of displaced circular orbit [au]
ψ = elevation angle [deg]
$\boldsymbol{\omega}$ = spacecraft angular velocity (with $\omega \triangleq \|\boldsymbol{\omega}\|$), [days^{-1}]
$\widetilde{\omega}$ = Keplerian orbit angular velocity, [days^{-1}]

Subscripts

max = maximum
min = minimum

Superscripts

$\bullet$ = time derivative
$\wedge$ = unit vector

1. Introduction

The concept of displaced non-Keplerian orbit (DNKO) can be traced back to Robert Forward [1] who, more than thirty years ago, suggested it as a potential commercial application of an advanced photonic solar sail-based spacecraft. The latter was assumed to be able to generate a geosynchronous orbit whose orbital plane was either above (northward) or below (southward) the terrestrial equatorial plane. Since then, displaced non-Keplerian orbits have been widely investigated in the field of solar sailing, as discussed in the comprehensive survey by McKay et al. [2]. In particular, McInnes [3] presented an essential overview of some mission applications by analyzing both the dynamics and the stability of DNKOs, Ceriotti et al. [4, 5, 6] investigated the possibility of using these orbits to obtain a "pole-sitter" mission (which means that the spacecraft is always placed above one of Earth's poles), whereas Heiligers et al. [7] recently extended the Forward's analysis to geosynchronous DNKOs maintained by a hybrid propulsion system (solar sail and solar electric thruster). In a heliocentric framework, MacDonald et al. [8] discussed the possibility of creating an interplanetary communications relay as a support for future explorations of Mars. Gong and Li [9, 10] analyzed the solar sail potentials of obtaining a heliocentric elliptic DNKO for planetary polar observation, and investigated the possibility of spin-stabilizing a spacecraft equipped with a solar sail on such an orbit. Recently, Song et al. [11] studied DNKOs for solar sails in the Hill's restricted three-body problem. In this context, Mengali and Quarta [12] presented a preliminary analysis of heliocentric circular DNKOs using an Electric Solar Wind Sail (E-sail) as the primary propulsion system, while Qi et al.[13] studied the optimization of transfer trajectories using a genetic algorithm.

The study of [12] is, however, based on a simplified mathematical model of the E-sail performance, for two main reasons. On one side the E-sail thrust modulus is assumed to vary with the Sun-spacecraft distance r as $1/r^{7/6}$. Actually, obtaining an accurate model of the E-sail thrust for mission analysis purposes is a complex task, due both to the variability of the solar wind properties, and to the difficulties in analyzing the interactions between the charged particles and the spacecraft artificial electric field. Nonetheless, numerical analyses based on accurate plasmadynamic simulations [14], which model the combined effect between the virtual decreasing of the electric field frontal area (proportional to $1/r^2$) and the increasing of the plasma Debye length (proportional to r), have shown that the thrust modulus scales as the inverse of the Sun-spacecraft distance. The second simplification introduced in [12] is that the thrust modulus is independent of the spacecraft attitude until the pitch angle α_n (the angle between the Sun-spacecraft line and the normal to the E-sail nominal plane in the direction opposite to the Sun) reaches a maximum value of about 60 deg–70 deg, while the cone angle α (the angle between the Sun-spacecraft line and the thrust direction) is one half of α_n and is, therefore, constrained to a maximum value of about 30 deg–35 deg.

In a recent paper, Yamaguchi and Yamakawa [15] proposed a refined mathematical model, in which the thrust modulus and the cone angle are both parameterized as functions of the E-sail attitude. This model has been derived from the numerical calculations of the thrust vectors acting on each conducting tether. In particular, the direction and the magnitude of the total thrust have been obtained as functions of the pitch

angle with a step-size of about 0.1 deg, and the results have been expressed in terms of best-fit polynomial equations.

The aim of this paper is to provide a reappraisal of circular heliocentric DNKOs and to improve the results of [12] using the thrust model by Yamaguchi and Yamakawa [15]. Different mission opportunities are discussed, obtained by changing the Sun-spacecraft distance, the orbital period and the spacecraft characteristic acceleration. The paper also includes an in depth discussion about the linear stability of DNKOs.

2. Mathematical Preliminaries

Consider a spacecraft S, propelled by an E-sail, at a distance r from the Sun. Let a_c be the spacecraft characteristic acceleration, which coincides with the maximum propulsive acceleration when $r = r_\oplus \triangleq 1\,\text{au}$. Let $\mathcal{P}$ be the plane that ideally contains the E-sail tethers, $\hat{\boldsymbol{n}}$ the unit vector normal to $\mathcal{P}$ in the direction opposite to the Sun. Also, let $\mathcal{R}$ be the local horizontal plane, that is, the plane containing S and orthogonal to the Sun-spacecraft line (which approximately coincides with the solar wind direction), and ℓ be a fixed reference line belonging to $\mathcal{R}$. The E-sail attitude is characterized by means of two angles: the pitch angle $\alpha_n \in [0,\, \pi/2]$, and the azimuthal angle $\delta_n \in [0,\, 2\,\pi]$, defined as the angle between the line ℓ and the projection of $\hat{\boldsymbol{n}}$ onto $\mathcal{R}$, see Fig. 2. Let $\hat{\boldsymbol{a}} \triangleq \boldsymbol{a}/\|\boldsymbol{a}\|$ be the propulsive acceleration unit vector, whose direction is defined through the cone angle $\alpha \in [0,\, \pi/2]$ (the angle between $\hat{\boldsymbol{a}}$ and the Sun-spacecraft line), and the clock angle $\delta \in [0,\, 2\,\pi]$ (the angle between the line ℓ and the projection of $\hat{\boldsymbol{a}}$ onto $\mathcal{R}$). Note that the direction of $\hat{\boldsymbol{a}}$ ranges between that of $\hat{\boldsymbol{n}}$ and $\hat{\boldsymbol{r}}$ (that is, $\alpha \le \alpha_n$), where $\hat{\boldsymbol{r}}$ is the spacecraft position unit vector. Since $\hat{\boldsymbol{a}}$ belongs to the plane spanned by $\hat{\boldsymbol{n}}$ and $\hat{\boldsymbol{r}}$, it turns out that $\delta = \delta_n$ and $\hat{\boldsymbol{a}}$ can be written as

$$\hat{\boldsymbol{a}} = \begin{cases} \dfrac{\sin(\alpha_n - \alpha)}{\sin\alpha_n}\,\hat{\boldsymbol{r}} + \dfrac{\sin\alpha}{\sin\alpha_n}\,\hat{\boldsymbol{n}} & \text{if} \quad \alpha_n \in (0,\, \pi/2] \\ \hat{\boldsymbol{r}} & \text{if} \quad \alpha_n = 0 \end{cases} \tag{1}$$

In the special case when plane $\mathcal{P}$ coincides with plane $\mathcal{R}$ (i.e. when $\alpha \equiv \alpha_n = 0$), then $\hat{\boldsymbol{n}} \equiv \hat{\boldsymbol{r}} = \hat{\boldsymbol{a}}$ and the clock angle δ is undefined.

In previous studies [16, 12] the simplified model of the E-sail performance was characterized by assuming $\alpha = \alpha_n/2$, with a maximum value of the cone angle $\alpha_{\max}$ of about 35 deg. Recently, Yamaguchi and Yamakawa [15] have shown that the function $\alpha = \alpha(\alpha_n)$ is more complex than a simple linear law, and can be accurately described by means of the following polynomial, which corresponds to a best-fit interpolation of numerical results

$$\alpha = b_6\,\alpha_n^6 + b_5\,\alpha_n^5 + b_4\,\alpha_n^4 + b_3\,\alpha_n^3 + b_2\,\alpha_n^2 + b_1\,\alpha_n + b_0 \tag{2}$$

where the coefficients b_i, with $i = 1, 2, \ldots, 6$, are summarized in Table 1. Note, in passing, that the coefficients in the table emend a couple of typos in [15].

i	0	1	2	3	4	5	6
b_i	0	4.853×10^{-1}	3.652×10^{-3}	-2.661×10^{-4}	6.322×10^{-6}	-8.295×10^{-8}	3.681×10^{-10}
c_i	1.000	6.904×10^{-5}	-1.271×10^{-4}	7.027×10^{-7}	-1.261×10^{-8}	1.943×10^{-10}	-5.896×10^{-13}

Table 1: Best-fit interpolation coefficients of thrust parameters (α and α_n in degrees). Data adapted from [15].

The variation of the cone angle α with the pitch angle α_n is shown in Fig. 1, from which the linear law turns out to be a good approximation of Eq. (2) until $\alpha_n \le 20\,\text{deg}$ (or $\alpha \le 10\,\text{deg}$). Figure 1 also shows that the maximum attainable value of the cone angle is slightly less than 20 deg, and it is reached when the pitch angle is about 55 deg. Such an extreme value of α, which quantifies the propulsion system capabilities of generating a transverse thrust, is significantly different from the value of 35 deg that has been used thus far for mission analysis purposes [16, 12].

The analysis of Yamaguchi and Yamakawa [15] also points out that, for a given Sun-spacecraft distance r, the propulsive acceleration modulus $\|\boldsymbol{a}\|$ is strongly dependent on the E-sail attitude through the pitch angle α_n. In fact, according to the procedure described in [15], if γ is the ratio between the modulus of

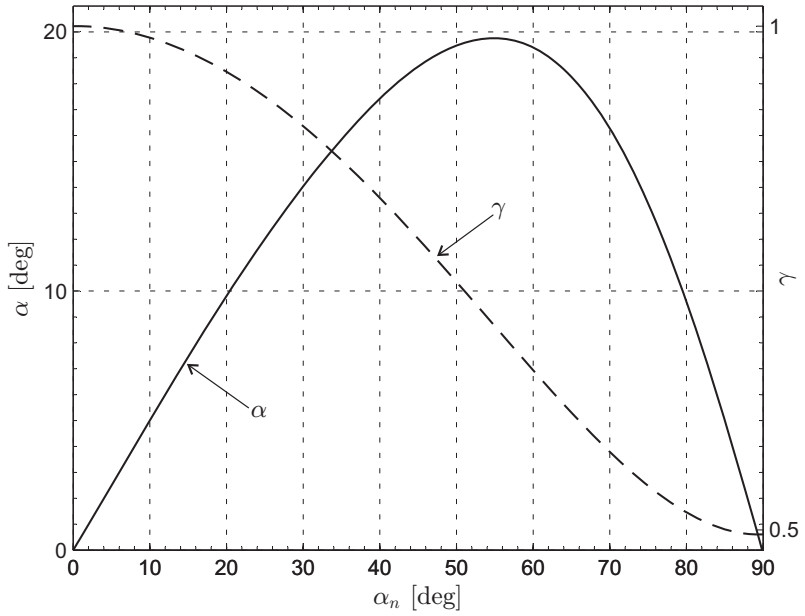

Figure 1: Cone angle α and dimensionless propulsive acceleration γ as a function of pitch angle α_n. Data adapted from [15].

the propulsive acceleration at an angle α_n to the maximum propulsive acceleration at a distance r from the Sun, or

$$\gamma \triangleq \frac{\|\boldsymbol{a}\|}{a_c\ (r_\oplus/r)} \tag{3}$$

then

$$\gamma = c_6\,\alpha_n^6 + c_5\,\alpha_n^5 + c_4\,\alpha_n^4 + c_3\,\alpha_n^3 + c_2\,\alpha_n^2 + c_1\,\alpha_n + c_0 \tag{4}$$

where the coefficients c_i, obtained again by numerical interpolation of simulation data, are summarized in Table 1. The variation of the dimensionless propulsive acceleration γ with the pitch angle is represented in Fig. 1 with dashed line. Note that γ varies between a maximum value of 1 when $\alpha_n = 0$ (i.e. when the E-sail nominal plane $\mathcal{P}$ is normal to the Sun-spacecraft line, or $\hat{\boldsymbol{n}} \equiv \hat{\boldsymbol{r}}$), and a minimum value of about 0.5 when $\alpha_n = 90\,\text{deg}$ (or $\hat{\boldsymbol{n}} \cdot \hat{\boldsymbol{r}} = 0$). Finally, combining Eqs. (1) and (3), the propulsive acceleration vector $\boldsymbol{a}$ can be written as

$$\boldsymbol{a} = \begin{cases} a_c\,\dfrac{r_\oplus}{r}\,\gamma\,\left[\dfrac{\sin\left(\alpha_n-\alpha\right)}{\sin\alpha_n}\,\hat{\boldsymbol{r}} + \dfrac{\sin\alpha}{\sin\alpha_n}\,\hat{\boldsymbol{n}}\right] & \text{if} \quad \alpha_n \in (0,\,\pi/2] \\ a_c\,\dfrac{r_\oplus}{r}\,\hat{\boldsymbol{r}} & \text{if} \quad \alpha_n = 0 \end{cases} \tag{5}$$

where $\cos\alpha_n = \hat{\boldsymbol{n}} \cdot \hat{\boldsymbol{r}}$.

2.1. Maintaining a circular DNKO

Consider an E-sail-based spacecraft moving along a heliocentric circular DNKO of radius ρ and center C, see Fig. 2 where $\mathcal{T}_\odot(O; x, y, z)$ is a heliocentric ecliptic Cartesian reference frame with origin O at the Sun's center-of-mass and unit vectors $\hat{\boldsymbol{\imath}}$, $\hat{\boldsymbol{\jmath}}$, and $\hat{\boldsymbol{k}}$.

Without loss of generality, assume that the spacecraft displaced orbital plane is parallel to the ecliptic plane (x, y). Let ω be the (constant) spacecraft angular velocity modulus, $T = 2\,\pi/\omega$ the orbital period, $\hat{\boldsymbol{\rho}}$ the radial unit vector whose direction is aligned, at any time, with the C-S line. Taking into account that the Sun-spacecraft distance r is constant (circular DNKO), the E-sail elevation angle $\psi \in [0,\,\pi/2]$, defined

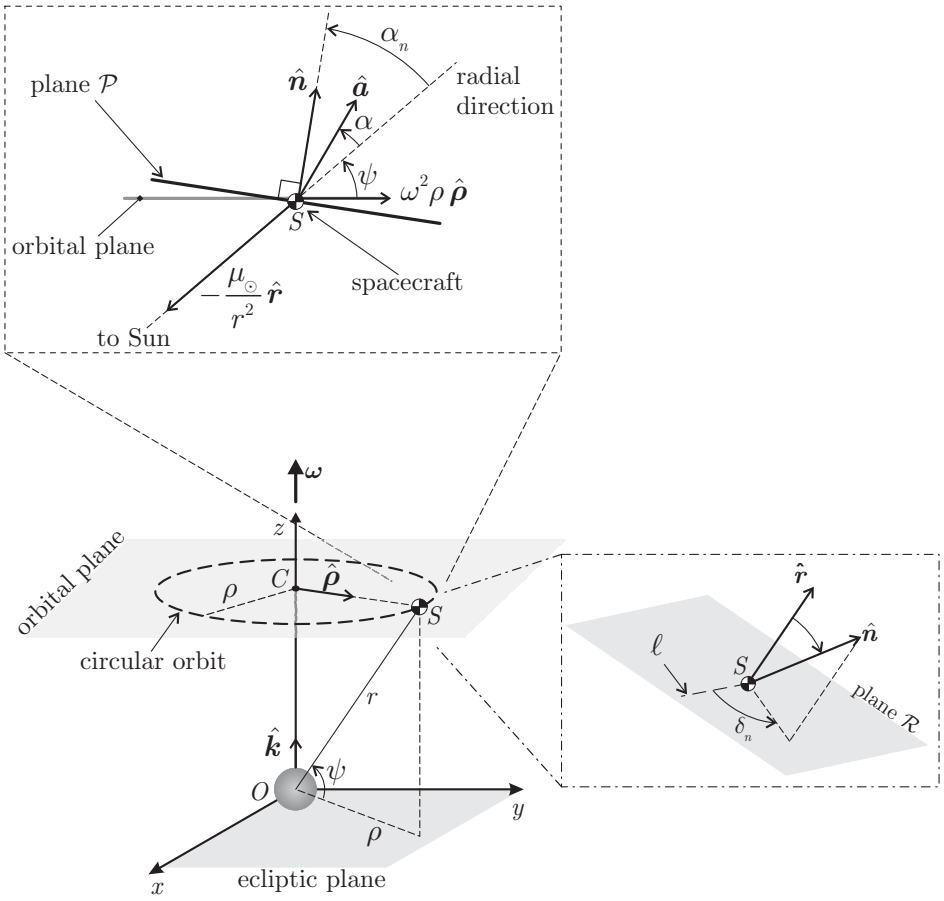

Figure 2: Layout of a circular heliocentric DNKO.

as the angle between the Sun-spacecraft line and the ecliptic plane, is a constant of motion given by the equation

$$\psi = \arccos\left(\frac{\rho}{r}\right) \tag{6}$$

Note that the case $\psi = 0$ (or $r = \rho$) corresponds to an ecliptic orbit, and the limit case $\psi = \pi/2$ refers to a spacecraft that levitates over the Sun's north pole (fixed heliocentric position, or heliostationary condition) along the z-axis of $\mathcal{T}_\odot$. For symmetry reasons, $\hat{\boldsymbol{a}}$ and $\hat{\boldsymbol{\rho}}$ must belong to the plane containing $\hat{\boldsymbol{k}}$ and $\hat{\boldsymbol{r}}$ in order to maintain a circular DNKO. In a general case in which the plane of the displaced orbit is not parallel to the ecliptic plane, $\hat{\boldsymbol{a}}$ and $\hat{\boldsymbol{\rho}}$ must belong, at any time, to the plane containing the unit vector $\hat{\boldsymbol{r}}$ and the O-C line, which coincides with the direction of the angular velocity vector $\boldsymbol{\omega}$.

A circular DNKO requires that the three accelerations acting on the spacecraft, that is, the gravitational ($-\mu_\odot\, \hat{\boldsymbol{r}}/r^2$), the centrifugal ($\omega^2\, \rho\, \hat{\boldsymbol{\rho}}$), and the propulsive ($\boldsymbol{a}$), be balanced. Bearing in mind Eq. (3) and Fig. 2, the two conditions necessary for maintaining a circular DNKO are

$$a_c\, \frac{r_\oplus}{r}\, \gamma\, \sin\alpha = \omega^2\, \rho\, \sin\psi \tag{7}$$

$$a_c\, \frac{r_\oplus}{r}\, \gamma\, \cos\alpha = \frac{\mu_\odot}{r^2} - \omega^2\, \rho\, \cos\psi \tag{8}$$

According to [17, 12] and taking into account Eqs. (7)-(8), the required cone angle α and characteristic

acceleration a_c are

$$\tan\alpha = \frac{(\omega/\widetilde{\omega})^2\ \tan\psi}{1+\tan^2\psi-(\omega/\widetilde{\omega})^2} \tag{9}$$

$$\frac{a_c}{\mu_\odot/r_\oplus^2} = \frac{r_\oplus}{r\,\gamma}\,f \tag{10}$$

where

$$f = f\left(\psi,\,\omega^2/\widetilde{\omega}^2\right) \triangleq \left(1-\frac{(\omega/\widetilde{\omega})^2}{1+\tan^2\psi}\right)\ \sqrt{1+\frac{\tan^2\psi}{[(1+\tan^2\psi)/(\omega/\widetilde{\omega})^2-1]^2}} \tag{11}$$

is an auxiliary function of $\left(\psi,\,\omega^2/\widetilde{\omega}^2\right)$, and

$$\widetilde{\omega} \triangleq \sqrt{\mu_\odot/r^3} \tag{12}$$

is the angular velocity of a reference Keplerian orbit with radius r. Recalling that α and γ are both function of the E-sail attitude via α_n, see Eqs. (2) and (4), Eqs. (9)-(10) relate the parameters describing the circular DNKO and the spacecraft performance in terms of characteristic acceleration and pitch angle.

It is now possible to summarize the procedure necessary to obtain a circular DNKO, whose geometry depends on parameters ψ, r and ω (the latter can be alternatively substituted by the period T). The required value of the cone angle α is obtained from Eq. (9), while the corresponding two admissible values of E-sail pitch angle are obtained by inverting Eq. (2) and taking the acceptable roots ($0 \leq \alpha_n \leq \pi/2$) or, equivalently, from Fig. 1. For each value of α_n, the dimensionless propulsive acceleration γ is calculated from Eq. (4), while the value of a_c is given by Eq. (10). As is discussed in the next section, the selection of α_n between the two admissible values influences the mission performance in terms of required characteristic acceleration.

3. Simulation results

A potential mission application is constituted by Type II DNKOs [17], that is, displaced orbits characterized by a period T equal to that of a Keplerian (circular) orbit of radius r. A spacecraft tracking such a trajectory could be able either to observe the polar regions of a celestial body with a small (heliocentric) orbital eccentricity, or to easily communicate with another spacecraft that covers a circular Keplerian (ecliptic) orbit. In this case $\omega = \widetilde{\omega}$, and Eq. (9) simplifies to

$$\tan\alpha = \frac{1}{\tan\psi} \tag{13}$$

which implies that α and ψ are complementary angles. Taking into account that $\alpha_{\max} \simeq 20\,\text{deg}$, see Fig. 1, the constraint of Eq. (13) makes Type II DNKOs feasible for large elevation angles only, i.e. approximately for $\psi > 70\,\text{deg}$, and for high characteristic accelerations, see Fig. 3. Note that, unlike [12], now there are two graphs for a given a_c since, according to the solid line of Fig. 1, a given value of the cone angle $\alpha \leq \alpha_{\max}$ can be obtained with two different values of the pitch angle, namely α_{n_1} and $\alpha_{n_2} \geq \alpha_{n_1}$. These two admissible values of α_n correspond to two different values of γ and, hence, to two different values of a_c, see Eq. (10). In particular, for a given Sun-spacecraft distance r, the required values of the characteristic acceleration are decreasing (or increasing) functions of angle ψ as long as the solution corresponding to α_{n_1} (or α_{n_2}) is considered.

In the previous analysis [12], the characteristic acceleration was an increasing function of ψ, and this behaviour was explained by the fact that an increasing elevation angle generates a greater component of gravitational force perpendicular to the (displaced) orbital plane, which must be balanced by the propulsive thrust. In this study, Fig. 3(a) shows a more complex behavior that can be explained by recalling that α and ψ are complementary angles for Type II DNKOs, see Eq. (13). Accordingly, an increasing value of ψ implies a decreasing value of α and, as long as the solution corresponding to α_{n_2} is considered, a greater value of the pitch angle. This, in its turn, leads to a smaller value of γ, see Fig. 1, and a higher value of required

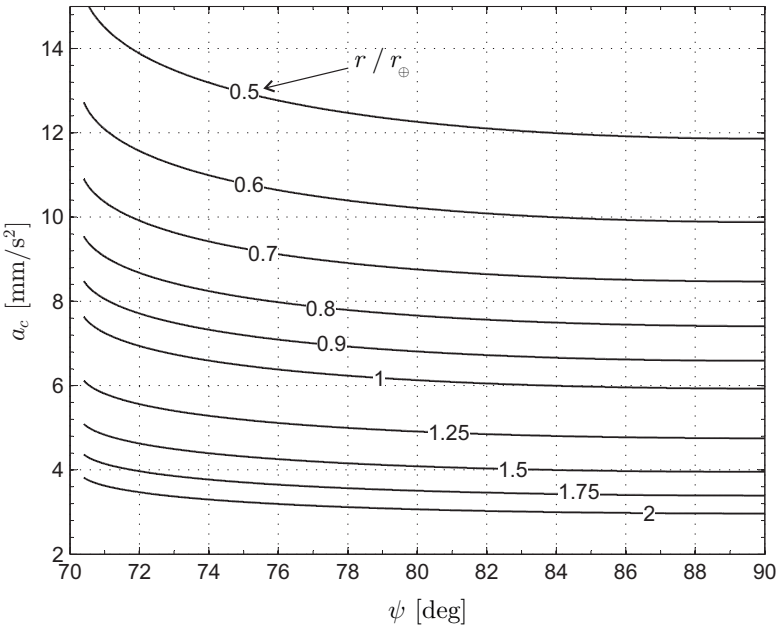

(a) Pitch angle α_{n_1}.

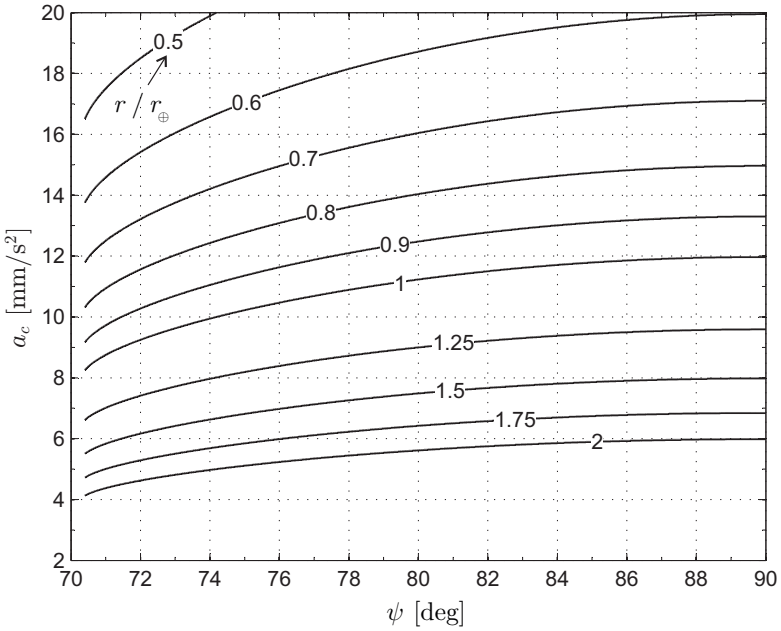

(b) Pitch angle $\alpha_{n_2} \geq \alpha_{n_1}$.

Figure 3: Characteristic acceleration required to maintain a Type II DNKO as a function of ψ and $r/r_\oplus$.

characteristic acceleration, see Fig. 3(b). On the other hand, when the solution α_{n_1} is selected, a decreasing value of α implies a decreasing value of pitch angle and a corresponding greater value of γ. The latter has a significative influence with respect to an increase of the gravitational force component perpendicular to the orbital plane and, therefore, the required characteristic acceleration for orbital maintenance with a larger elevation angle is smaller, as is shown in Fig. 3(a). Note that $\gamma(\alpha_{n_1})$, i.e. the value of γ obtained with α_{n_1}, is always greater than $\gamma(\alpha_{n_2})$: therefore the solution corresponding to α_{n_1} is the most convenient in terms of propulsive requirements. However, even in the most favourable case ($\alpha_n = \alpha_{n_1}$), a Type II DNKO at a Sun distance of about $r_\oplus$, requires a characteristic acceleration greater than $6\,\mathrm{mm/s^2}$, a value well beyond the current capabilities of an E-sail.

Figure 4 shows a comparison between the results of [12] and those obtained using the thrust model of [15], when $\alpha_n = \alpha_{n_1}$. Note that for $r < 1\,\mathrm{au}$ the thrust model of [15] provides a greater value of characteristic acceleration required for orbital maintenance. For $r > 1\,\mathrm{au}$, instead, the model of [15] may produce lower propulsive requirements with respect to the previous ones, because of the exponent of $1/r$ in the thrust formula (especially when large values of elevation angle are considered).

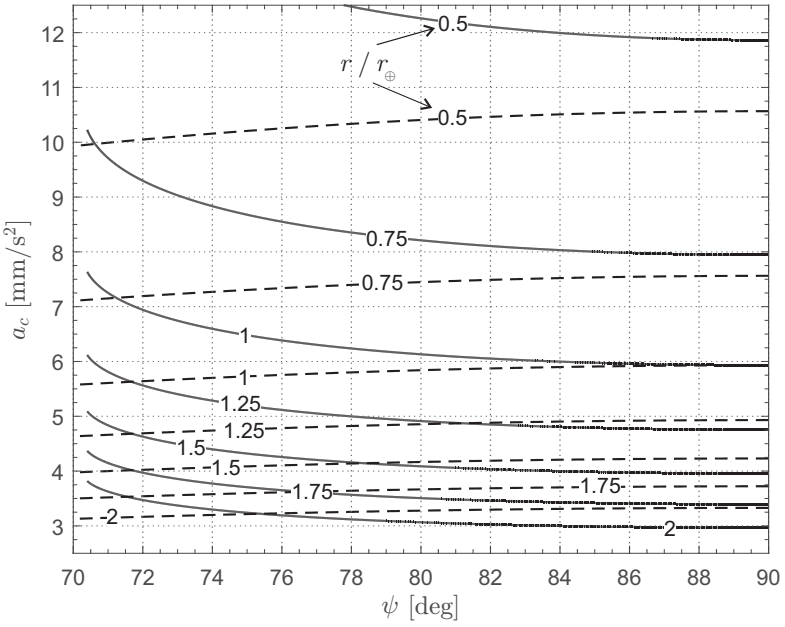

Figure 4: Characteristic acceleration required to maintain a Type II DNKO as a function of ψ and $r/r_\oplus$. Thrust model of [15] (continuous line) vs. original (dashed line).

An interesting case is obtained when the elevation angle ψ is zero, that is, when the orbits belong to the ecliptic plane. In fact, the condition $\psi = 0$ implies $\alpha = 0$ from Eq. (7) and, therefore, Eq. (8) can be rearranged as

$$\frac{a_c}{\mu_\odot / r_\oplus^2} = \frac{1}{\gamma}\left(\frac{r_\oplus}{r}\right)\left[1 - \left(\frac{\omega}{\widetilde{\omega}}\right)^2\right] \tag{14}$$

where the admissible values of the dimensionless propulsive acceleration are $\gamma_{\max} = 1$ and $\gamma_{\min} \simeq 0.5$. In this scenario, for a given pair $\{r, \omega\}$, Eq. (14) gives two values of characteristic acceleration that guarantee orbital maintenance. The solution corresponding to a lower α_n (and therefore to a greater γ) is the most convenient, whereas the two values of a_c coalesce in a double solution ($a_c = 0$) when $\omega = \widetilde{\omega} = \sqrt{\mu_\odot / r^3}$, i.e. for a circular Keplerian orbit. In this case the differences, in terms of performance, between original [12] and recent [15] thrust models are due only to the change in the exponent of $1/r$ (which varies from 7/6 to 1) in the propulsive acceleration formula. In the model of [15], the required value of characteristic acceleration is smaller (greater) for $r > 1\,\mathrm{au}$ ($r < 1\,\mathrm{au}$) with respect to the original results, see Fig. 5.

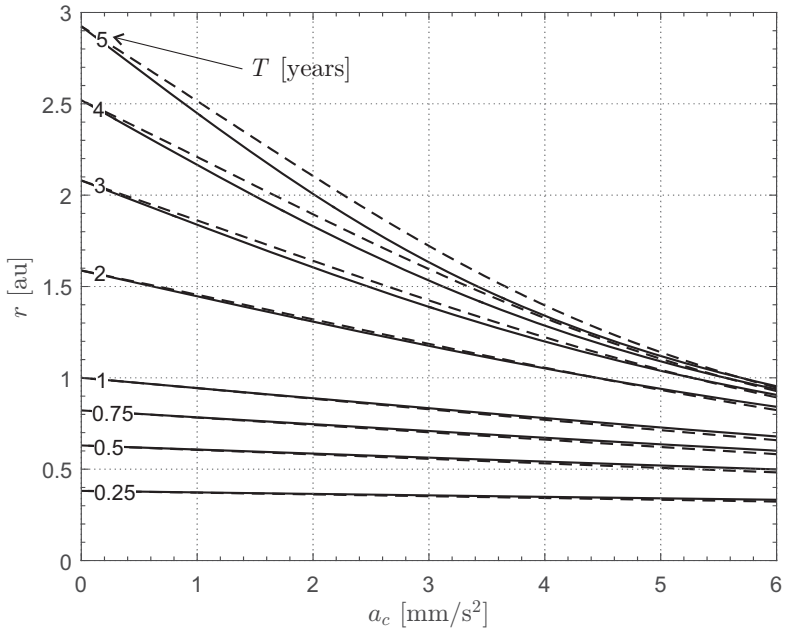

Figure 5: Heliocentric radius r of ecliptic circular orbit ($\psi = 0$) as a function of a_c and T. Thrust model of [15] (continuous line) vs. original (dashed line).

The last potential mission application refers to the case in which $\psi = 90\,\text{deg}$, that is, when the circular orbit degenerates in a single point placed on the z-axis of $\mathcal{T}_\odot$. In this scenario the spacecraft inertial position is fixed, and the E-sail levitates over the Sun's pole at a distance r_l that can be found by enforcing the equilibrium between the gravitational force and the propulsive thrust, viz.

$$r_l = \frac{\mu_\odot}{a_c\, r_\oplus\, \gamma} \tag{15}$$

Note that Eq. (15) is a special case of Eq. (8) when $\psi = 90\,\text{deg}$, and that the heliostationary condition can be obtained only with a radial propulsive acceleration in which $\alpha = 0$ and $\gamma = \{\gamma_{\min}, \gamma_{\max}\}$, see Fig. 1. For a given value of heliostationary distance r_l, the minimum required value of a_c is obtained when $\gamma = \gamma_{\max} = 1$. The performance variation compared to the model used in [12] is, again, due to the different propulsive variation law with the distance r. In particular, the model of [15] shows that, the characteristic acceleration being the same, the heliostationary condition can be attained at a smaller distance if $r > 1\,\text{au}$, see Fig. 6.

4. Linear stability analysis

Having discussed the E-sail performance necessary to maintain a Type II DNKO, an important point involves the question of whether those orbits are stable or not. This problem will now be addressed by confining the discussion to the linear stability case. To clarify the discussion, it is useful to first investigate the particular cases of $\psi = 90\,\text{deg}$ and $\psi = 0\,\text{deg}$. The simplest situation corresponds to the heliostationary condition ($\psi = 90\,\text{deg}$), when the E-sail motion around the equilibrium (heliostationary) point is described by the differential equation

$$\ddot{r} = -\frac{\mu_\odot}{r^2} + \frac{r_\oplus}{r}\, a_c\, \gamma \tag{16}$$

where the dot symbol represents a derivative taken with respect to the time. Note that, according to Eq. (15), the equilibrium distance $r_0 \equiv r_l$ is found by setting $\ddot{r} = 0$ in the preceding equation.

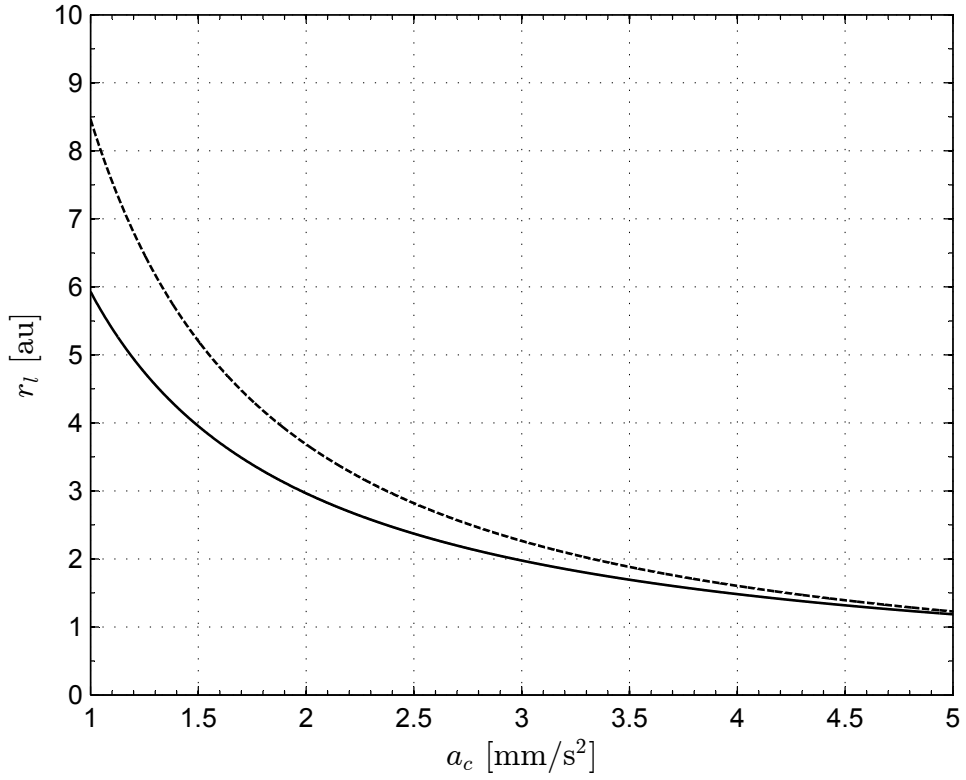

Figure 6: Heliostationary distance r_l as a function of a_c. Thrust model of [15] (continuous line) vs. original (dashed line).

The linearized dynamics of perturbation motion is obtained by using the transformation $r = r_0(1 + \delta)$, where $\delta \ll 1$ is the dimensionless distance variation along the radial direction, and the result is

$$\ddot{\delta} - \frac{\mu_\odot}{r_0^3}\delta = 0 \tag{17}$$

that shows the (linear) instability of the perturbation motion. Note that Eq. (17) can be rewritten in a dimensionless form by introducing the dimensionless time $\tau \triangleq \widetilde{\omega}\, t$, where $\widetilde{\omega}$ is given by Eq. (12) with $r = r_0$, as

$$\delta'' - \delta = 0 \tag{18}$$

where the prime symbol denotes a derivative with respect to τ.

Consider now the case of a circular orbit belonging to the ecliptic plane ($\psi = 0$). From Eq. (7), the cone angle is zero and, therefore, the propulsive thrust is purely along the radial direction. Accordingly, the spacecraft motion is described by the differential equation

$$\ddot{r} = -\frac{\mu_\odot}{r^2} + \frac{r_\oplus}{r} a_c \gamma + \frac{h^2}{r^3} \tag{19}$$

where the last term is the centrifugal acceleration along the circular orbit of (given) angular velocity $\omega = h/r^2$, with h being the (constant) orbital angular momentum. The equilibrium condition, obtained when $\ddot{r} = 0$, provides

$$a_{c_0} = \frac{\mu_\odot}{r_0\, r_\oplus\, \gamma} - \frac{h^2}{r_0^2\, r_\oplus\, \gamma} \tag{20}$$

which is in agreement with Eq. (8) when $\alpha = \psi = 0$. Substituting $r = r_0(1 + \delta)$ into Eq. (19), the corresponding linearized dynamics of perturbation motion is

$$\ddot{\delta} + \left(2\,\frac{h^2}{r_0^4} - \frac{\mu_\odot}{r_0^3}\right)\delta + p = 0 \tag{21}$$

where p is a constant, depending on the initial conditions on the perturbed ecliptic orbit, which does not affect the stability analysis. Equation (21) is more conveniently rewritten in dimensionless terms as

$$\delta'' + \left(2\,\frac{\omega^2}{\widetilde{\omega}^2} - 1\right)\delta + \frac{p}{\widetilde{\omega}^2} = 0 \tag{22}$$

The motion is therefore stable when

$$\frac{\omega^2}{\widetilde{\omega}^2} > \frac{1}{2} \tag{23}$$

According to Eq. (23), a Type II orbit belonging to the ecliptic plane is therefore stable.

The linear stability of DNKOs for a generic value of ψ is more involved, and is now discussed under the assumption that the cone angle α remains constant. The spacecraft equations of motion along the directions of $\hat{\boldsymbol{\rho}}$ and $\hat{\boldsymbol{k}}$ are

$$\ddot{\rho} = -\frac{\mu_\odot}{r^3}\,\rho + \frac{r_\oplus}{r} a_c\,\gamma\,\cos(\alpha+\psi) + \frac{h^2}{r^2\,\rho} \tag{24}$$

$$\ddot{z} = -\frac{\mu_\odot}{r^3}\,z + \frac{r_\oplus}{r} a_c\,\gamma\,\sin(\alpha+\psi) \tag{25}$$

Note that the two equilibrium conditions, obtained by setting $\ddot{\rho} = 0$ and $\ddot{z} = 0$, are equivalent to those given by Eqs. (7) and (8). Paralleling the previously discussed approach, the linearized dynamics of perturbation motion is obtained with the substitution $\boldsymbol{r} = \boldsymbol{r}_0 + \mathrm{d}\boldsymbol{r}$, with $\mathrm{d}\boldsymbol{r} = r_0[\delta_\rho,\, 0,\, \delta_z]^{\mathrm{T}}$. A perturbation in the transverse direction would simply imply a different angular coordinate on the nominal orbit, but does not affect its stability. Accordingly, the second component of $\mathrm{d}\boldsymbol{r}$ is set equal to zero. After some calculations, which are omitted for the sake of conciseness, the linearized dynamics of perturbation motion can be shown to be described by the following dimensionless equations

$$\delta_\rho'' = a_{11}\delta_\rho + a_{12}\delta_z + q \tag{26}$$

$$\delta_z'' = a_{21}\delta_\rho + a_{22}\delta_z \tag{27}$$

where q is a constant depending on the initial conditions. The coefficients a_{ij} are defined as

$$a_{11} = 3\,\cos^2\psi - 1 - \left(\omega^2/\widetilde{\omega}^2\right)\left(2\cos^2\psi + 1\right) - \cos(\alpha+2\psi)\,f \tag{28}$$

$$a_{12} = 3\,\cos\psi\,\sin\psi - (\omega^2/\widetilde{\omega}^2)\sin(2\psi) - \sin(\alpha+2\psi)\,f \tag{29}$$

$$a_{21} = 3\,\cos\psi\,\sin\psi - \sin(\alpha+2\psi)\,f \tag{30}$$

$$a_{22} = 3\,\sin^2\psi - 1 + \cos(\alpha+2\psi)\,f \tag{31}$$

where f is given by Eq. (11) and α is obtained from Eq. (9). Note that all of the four coefficients a_{ij} depend on the pair $(\psi,\, \omega^2/\widetilde{\omega}^2)$, and so the linear stability of the perturbation motion. The previously discussed special cases of $\psi = 90\,\mathrm{deg}$ and $\psi = 0\,\mathrm{deg}$ can both be recovered from Eqs. (26)-(27). In fact, $\psi = 90\,\mathrm{deg}$ (and $\alpha = 0$) corresponds to $\omega = 0$ and $f = 1$, which implies $a_{21} = 0$ and $a_{22} = 1$. Therefore Eq. (27) reduces to Eq. (18). Likewise, if $\psi = 0$ (and, again, $\alpha = 0$), then $f = 1 - \omega^2/\widetilde{\omega}^2$, which implies $a_{11} = 1 - 2\,\omega^2/\widetilde{\omega}^2$ and $a_{12} = 0$. Accordingly, Eq. (26) reduces to Eq. (22).

Using the Laplace transformation, the characteristic equation associated to the system of differential equations (26)-(27) is

$$s^4 + b\,s^2 + c = 0 \tag{32}$$

where

$$b \triangleq -\left(a_{11} + a_{22}\right) \tag{33}$$

$$c \triangleq a_{11}\,a_{22} - a_{12}\,a_{21} \tag{34}$$

Since the characteristic equation is biquadratic, if $\bar{s}$ is a root of Eq. (32), so is $-\bar{s}$. Therefore, the linear stability of the perturbation motion requires that all roots of Eq. (32) be imaginary. Equivalently, the three conditions that guarantee a stable motion are $b > 0$, $c > 0$, and $b^2 - 4\,c > 0$ (the latter is always met

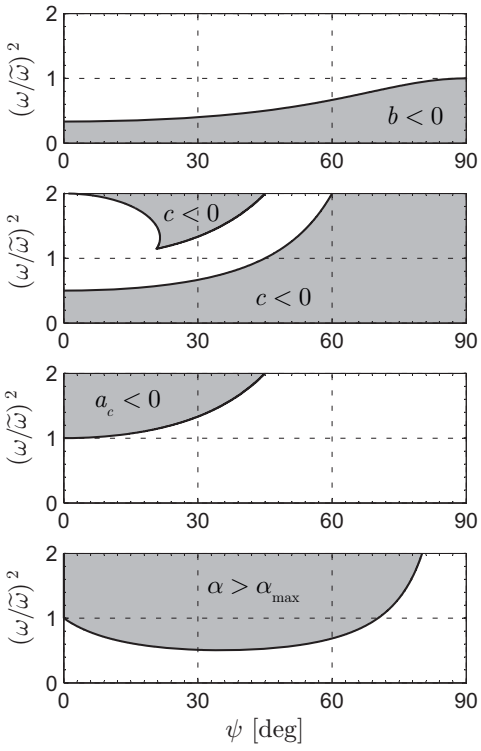

Figure 7: Map of stability/feasibility conditions (grey regions are unfeasible and/or unstable).

according to the simulations). Figure 7 shows the regions of the plane $(\psi, \omega^2/\widetilde{\omega}^2)$ where the two remaining stability conditions, $b > 0$ and $c > 0$, are met. It also shows the region of unfeasible points due to either a negative value of the characteristic acceleration ($a_c < 0$) or to a cone angle that exceeds the maximum admissible value ($\alpha > \alpha_{\max}$). These data are collected in a single plot, see Fig. 8, which shows the admissible region as a function of the elevation angle. In particular, note that a Type II DNKO is stable only when it belongs to the equatorial plane.

5. Conclusions

Electric solar wind sails are theoretically capable of maintaining a number of displaced non-Keplerian orbits by orienting the thrust vector in such a way that gravitational and centrifugal forces are balanced. The analysis of this paper confirms that, even using a refined mathematical model that takes into accounts the variations of thrust modulus and direction with the spacecraft attitude, the achievement of displaced circular orbits with a high elevation angle and a small heliocentric distance is still beyond the capabilities of the current technology. This problem could probably be mitigated by considering an oscillating cylindrically-constrained non-Keplerian orbit, thus extending to an electric sail a similar analysis available, in the literature, for a photonic solar sail. Moreover, displaced orbits are unstable when the elevation angle exceeds about 20 deg and, in that case, an active control strategy is necessary to maintain the trajectory.

Although the new thrust model is suitable for a preliminary mission analysis, it neglects the variability of the solar wind characteristics assuming the presence of a closed loop control system capable of continuously adjusting the tether voltage, in order to properly modulate the thrust intensity. Further improvements are therefore advisable and could be obtained by taking into account the effects of a space-temporal variation of the physical characteristics of the solar wind.

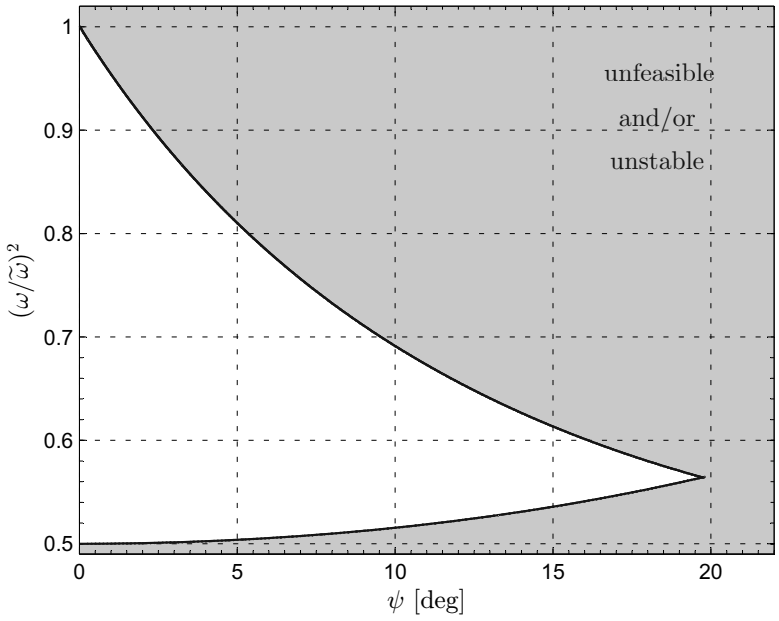

Figure 8: Admissible region for DNKOs.

References

[1] R. L. Forward, Light-levitated geostationary cylindrical orbits using perforated light sails, Journal of the Astronautical Sciences 32 (1984) 221–226 .

[2] R. J. McKay, M. Macdonald, J. D. Biggs, C. R. McInnes, Survey of highly-non-keplerian orbits with low-thrust propulsion, Journal of Guidance, Control, and Dynamics 34 (3) (2011) 645–666, doi: 10.2514/1.52133.

[3] C. R. McInnes, Dynamics, stability, and control of displaced non-keplerian orbits, Journal of Guidance, Control, and Dynamics 21 (5) (1998) 799–805, doi: 10.2514/2.4309.

[4] M. Ceriotti, C. R. McInnes, B. L. Diedrich, The pole-sitter mission concept: An overview of recent developments and possible future applications, in: 62nd International Astronautical Congress, Vol. 3, Cape Town, South Africa, 2011, pp. 2543–2559.

[5] M. Ceriotti, C. R. McInnes, Systems design of a hybrid sail pole-sitter, Advances in Space Research 48 (11) (2011) 1754–1762, doi: 10.1016/j.asr.2011.02.010.

[6] M. Ceriotti, J. Heiligers, C. R. McInnes, Trajectory and spacecraft design for a pole-sitter mission, Journal of Spacecraft and Rockets 51 (1) (2014) 311–326, doi: 10.2514/1.A32477.

[7] J. Heiligers, M. Ceriotti, C. R. McInnes, J. D. Biggs, Displaced geostationary orbit design using hybrid sail propulsion, Journal of Guidance, Control, and Dynamics 34 (6) (2011) 1852–1866, doi: 10.2514/1.53807.

[8] M. MacDonald, R. J. McKay, M. Vasile, F. De Frescheville, J. D. Biggs, C. R. McInnes, Low-thrust-enabled highly-non-keplerian orbits in support of future mars exploration, Journal of Guidance, Control, and Dynamics 34 (5) (2011) 1396–1411, doi: 10.2514/1.52602.

[9] S. Gong, J. Li, Solar sail heliocentric elliptic displaced orbits, Journal of Guidance, Control, and Dynamics 37 (6) (2014) 2021–2025, doi: 10.2514/1.G000660.

[10] S. Gong, J. Li, Spin-stabilized solar sail for displaced solar orbits, Aerospace Science and Technology 32 (1) (2014) 188–199, doi: 10.1016/j.ast.2013.10.002.

[11] M. Song, X. He, D. He, Displaced orbits for solar sail equipped with reflectance control devices in hill's restricted three-body problem with oblateness, Astrophysics and Space Science 361 (10), doi: 10.1007/s10509-016-2915-9.

[12] G. Mengali, A. A. Quarta, Non-keplerian orbits for electric sails, Celestial Mechanics and Dynamical Astronomy 105 (1–3) (2009) 179–195, doi: 10.1007/s10569-009-9200-y.

[13] N. Qi, M. Huo, Q. Yuan, Displaced electric sail orbits design and transition trajectory optimization, Mathematical Problems in Engineering 2014, doi: 10.1155/2014/932190.

[14] P. Janhunen, The electric solar wind sail status report, in: European Planetary Science Congress 2010, Vol. 5, European Planetology Network and the European Geosciences Union, 2010, paper EPSC 2010-297.

[15] K. Yamaguchi, H. Yamakawa, Study on orbital maneuvers for electric sail with on-off thrust control, Aerospace Technology Japan, the Japan Society for Aeronautical and Space Sciences 12 (2013) 79–88, doi: 10.2322/astj.12.79.

[16] G. Mengali, A. A. Quarta, P. Janhunen, Electric sail performance analysis, Journal of Spacecraft and Rockets 45 (1) (2008) 122–129, doi: 10.2514/1.31769.

[17] C. R. McInnes, Solar Sailing: Technology, Dynamics and Mission Applications, Space Science and Technology, Springer-Verlag, Berlin, 2004, pp. 173–180, ISBN: 978-3540210627.